Hole-Doped Semiconductor Nanowire on Top of an s-Wave Superconductor: A New and Experimentally Accessible System for Majorana Fermions

Li Mao, Ming Gong, E. Dumitrescu, Sumanta Tewari, and Chuanwei Zhang

Phys. Rev. Lett. **108**, 177001 — Published 24 April 2012

DOI: 10.1103/PhysRevLett.108.177001

Hole-doped semiconductor nanowire on top of an *s*-wave superconductor: A new and experimentally accessible system for Majorana fermions

Li Mao[1], Ming Gong[1], E. Dumitrescu[2], Sumanta Tewari[2], and Chuanwei Zhang[1*]
[1]*Department of Physics and Astronomy, Washington State University, Pullman, WA 99164 USA*
[2]*Department of Physics and Astronomy, Clemson University, Clemson, SC 29634 USA*

Majorana fermions were envisioned by E. Majorana in 1935 to describe neutrinos. Recently it has been shown that they can be realized even in a class of electron-doped semiconductors, on which ordinary *s*-wave superconductivity is proximity induced, provided the time reversal symmetry is broken by an external Zeeman field above a threshold. Here we show that in a hole-doped semiconductor nanowire the threshold Zeeman field for Majorana fermions can be very small for some *magic* values of the hole density. In contrast to the electron-doped systems, smaller Zeeman fields and much stronger spin-orbit coupling and effective mass of holes allow the hole-doped systems to support Majorana fermions in a parameter regime which is routinely realized in current experiments.

PACS numbers: 74.78.-w, 03.67.Lx, 71.10.Pm, 74.45.+c

Recently some exotic condensed matter systems, such as the Pfaffian states in fractional quantum Hall systems [1–4], chiral *p*-wave superconductors/superfluids [5–9], *etc.* [10, 11], have been proposed as systems supporting quasiparticles non-Abelian exchange statistics [12]. These systems allow a special type of quasiparticles called Majorana fermions which are their own anti-particles and possess the non-Abelian statistics. Due to the fundamental difference of Majorana fermions from any other known quantum particles in nature, the emergence of these particles in solid state systems would in itself be an extraordinary phenomenon. Their potential use in fault-tolerant topological quantum computation (TQC) [12] makes their realization in controllable solid state systems even more significant.

It has been shown recently [13–18] that an electron-doped semiconducting thin film or nanowire with a sizable spin-orbit coupling can host, under suitable conditions, Majorana fermion excitations localized near defects. This proposal followed on an earlier similar proposal in the context of cold atomic systems [19]. When the film or the nanowire is in the presence of a Zeeman splitting V_z (with Landé factor g_e^*) and an *s*-wave superconducting pair potential Δ, which can be proximity induced by a nearby superconductor, the system enters into a topological superconducting (TS) state for

$$V_z^2 > \Delta^2 + \mu^2, \quad V_z = g_e^* \mu_B B/2. \tag{1}$$

Here μ is the chemical potential in the semiconductor. Despite the theoretical success, the above requirement for the TS state in an electron-doped nanowire leads to two obvious experimental challenges: a low electron density and a high magnetic field. For a small carrier density a nanowire tends to become insulating due to the strong disorder-induced fluctuations of the chemical potential. A high magnetic field, on the other hand, can be detrimental to pairing as well as *s*-wave proximity effect itself.

In this Letter we show that a *hole-doped* semiconductor nanowire can solve all these problems encountered in the electron-doped systems. The hole-doped nanowire is very different in many respects from its electron-doped counterpart due to its different band structure and the value of the effective spin of the carriers. For some "magic" values of the carrier (hole) density the threshold Zeeman splitting for the TS states and Majorana fermions can become very small, therefore the constraint on the carrier density as given in Eq. (1) is absent for the hole-doped nanowires. Furthermore, the effective mass and spin-orbit coupling in the *p*-type *valence* band holes are much larger than electrons, which leads to a larger Fermi vector k_F. This larger k_F leads to a larger required carrier density ($\sim 10^6$ cm^{-1}) for the TS state, which, remarkably, is now *routinely achieved* in many experiments [20–22]. The large carrier density provides strong screening of the disorder potentials, leading to much smaller fluctuations of the chemical potential [23] in the nanowire. Furthermore, the small ratio between the Zeeman coupling and the spin-orbit energy (orders of magnitude smaller than that in the electron-doped systems) leads to a small carrier mobility requirement for the hole-doped TS state (3 order of magnitude smaller than that for the electron-doped TS state) [24]. Let us also point out that the superconducting proximity effect on a hole-doped nanowire has been observed in recent experiments [22]. It seems therefore that a Majorana-carrying TS state is tantalizingly close to experimental reach in a hole-doped nanowire.

Set-up and Hamiltonian: The experimental setup is illustrated in Fig. 1a, where a hole-doped semiconductor nanowire is placed on top of an *s*-wave superconductor. The single particle Hamiltonian of holes is described by the four-band Luttinger model [25] (henceforth we set $\hbar = 1$, and $m = -1$),

$$H_L = (\frac{\gamma_1}{2} + \frac{5\gamma_2}{4})\nabla^2 - \gamma_2(\nabla \cdot \mathbf{J})^2 - i\alpha(\mathbf{J} \times \nabla) \cdot \hat{z} + V_z J_z - \mu, \tag{2}$$

where α is the Rashba spin-orbit coupling, and the fourth term is the Zeeman field $V_z = g_h^* \mu_B B$ generated by the external magnetic field. $\mathbf{J}$ is the total angular momentum

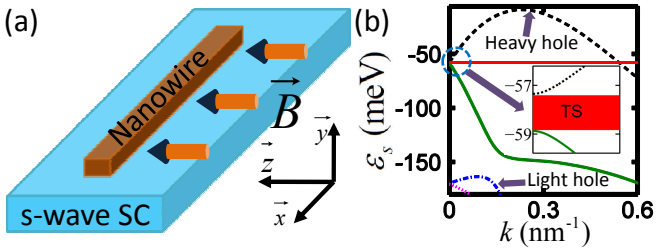

FIG. 1: (a) Schematic plot of the experimental setup. (b) The valence band structure of 1D hole-doped nanowire with a Zeeman field. Dashed and solid lines: heavy hole bands. Dash-dotted and dotted lines: light hole bands. Thick red line (amplified as shadow in inset): the regime for the topological superconducting state. The parameters are for a hole-doped InAs nanowire with $\gamma_1 = 20$, $\gamma_2 = 8.5$. $\alpha = 3.3 \times 10^5$ m/s, $V_z = 1.5$ meV, $L_z = 14$ nm, $L_y = 10$ nm.

operator for a spin-3/2 hole, γ_1 and γ_2 are the Luttinger parameters. Note that here the relation between V_z and B differs from Eq. (1) by a factor 1/2 because we use the spin-3/2 matrix J_z, instead of the Pauli matrix which was used for Eq. (1) [13] (thus the required B for the same V_z is smaller by a factor 1/2).

To simplify the calculations we assume a rectangular cross-section of the nanowire with the widths L_y and L_z. The strong confinement along the y and z directions makes the energy levels quantized on these axes. To illustrate the emergence of the Majorana fermions, we first consider only the lowest energy state along the y and z directions, on which the original 3D Hamiltonian (2) can be projected to an effective 1D form

$$\begin{aligned} H_1(x) &= \left(\gamma_1/2 + 5\gamma_2/4 - \gamma_2 J_x^2\right)\partial_x^2 + \pi^2\gamma_2 J_y^2/L_y^2 \\ &\quad + \pi^2\gamma_2 J_z^2/L_z^2 + i\alpha J_y\partial_x + V_z J_z - \xi - \bar{\mu}, \end{aligned} \quad (3)$$

where $\xi = 5\gamma_2\pi^2\left(L_y^{-2} + L_z^{-2}\right)/4$, and the shifted chemical potential $\bar{\mu} = \mu + \gamma_1\pi^2\left(L_y^{-2} + L_z^{-2}\right)/2$.

In Fig. 1b, we plot the energy spectrum ε_S of the Hamiltonian (3). There are two heavy hole and two light hole bands. If μ lies in the shaded region, it intercepts only one Fermi surface. An odd number of Fermi surfaces implies a breakdown of the fermion doubling theorem (due, in this case, to the Zeeman splitting), which yields, in the presence of a superconducting pair potential, the required TS state for Majorana fermions [10]. The position and width of the shaded region (the TS state) are determined by the Hamiltonian (3) at $k = 0$ (depends on the parameters γ_1, γ_2, L_y, L_z) and V_z, respectively. The large effective mass and strong spin-orbit coupling of the holes lead to a high density $n = \int_0^{k_F} dk/2\pi \sim 10^6$ cm^{-1} of holes in the TS state, which is routinely realized in nanowire experiments [20–22].

The superconducting pair potential can be induced in the hole-doped nanowire through the proximity contact with an s-wave superconductor (Fig. 1a), as demonstrated in experiments [22]. This yields the Hamiltonian,

$$H_{sc} = \sum\nolimits_{m_J} \int d^3\mathbf{r}\Delta_{sm_J}(\mathbf{r})\,\hat{\psi}^\dagger_{m_J}\hat{\psi}^\dagger_{-m_J} + \text{H.c.}, \quad (4)$$

where $\hat{\psi}^\dagger_{m_J}$ are the creation operators for holes with the angular momentum $m_J = \frac{1}{2}, \frac{3}{2}$ and $\Delta_{sm_J}(\mathbf{r})$ is the proximity induced pair potential. The form of the pairing Hamiltonian is dictated by the fact that Δ_{sm_J} couples particles with m_J with particles with $-m_J$, and should be determined through the microscopic theory of the proximity effect [26].

Taking account of the spin-3/2 and the particle-hole degrees of freedom in the superconductor, the Bogoliubov-de-Gennes (BdG) Hamiltonian can be written as an 8×8 matrix

$$\hat{H}_{\text{BdG}} = \begin{pmatrix} H_1(x) & \Delta_S(x) \\ \Delta_S^*(x) & -\Upsilon^\dagger H_1^*(x)\Upsilon \end{pmatrix} \quad (5)$$

in the Nambu spinor basis $\hat{\Phi}(x) = \left(\hat{\psi}(x), \Upsilon\hat{\psi}^\dagger(x)\right)^T$ with $\Upsilon = i(I_2 \otimes \sigma_x)\tau_y$ (I_2 is the 2×2 unit matrix), $\Delta_S(x) = \text{diag}\left(\Delta_{s3/2}, \Delta_{s1/2}, \Delta_{s1/2}, \Delta_{s3/2}\right)$, and $\hat{\psi}(x) = (\hat{\psi}_{\frac{3}{2}}(x), \hat{\psi}_{\frac{1}{2}}(x), \hat{\psi}_{-\frac{1}{2}}(x), \hat{\psi}_{-\frac{3}{2}}(x))$.

Parameter space for the topological state: In a 1D nanowire, the parameter regime for the Majorana fermions can be determined by the topological index $\mathcal{M}$ [27, 28] defined as,

$$\mathcal{M} = \text{sgn}\left[\text{Pf}\left\{\Gamma(0)\right\}\right]\text{sgn}\left[\text{Pf}\left\{\Gamma(\pi/a)\right\}\right]. \quad (6)$$

Here Pf represents the Pfaffian of the anti-symmetric matrix $\Gamma(k) = -iH_{\text{BdG}}(k)(\varsigma_y \otimes \Upsilon)$, ς_y is the Pauli matrix, $H_{\text{BdG}}(k)$ is the corresponding BdG Hamiltonian in the momentum space ($-i\partial_x \to k$), and a is the lattice constant. $\mathcal{M} = -1$ ($+1$) corresponds to the topologically nontrivial (trivial) states with (without) Majorana fermions. Using the fact that $\Gamma(k)$ is an anti-symmetric matrix that can be diagonalized by a lower triangular matrix [29], we find

$$\text{Pf}\left\{\Gamma(k)\right\} = \text{Pf}\left\{\Delta_S\Upsilon\right\}\text{Pf}\left\{\Upsilon\Delta_S + H_1^T(k)\,\Upsilon\Delta_S^{-1}H_1(k)\right\}. \quad (7)$$

In the continuous limit $k = \pi/a \to \infty$, the k^2 terms in $H_1(k)$ dominates and all other terms in $\Gamma(k)$ can be neglected, yielding $\text{sgn}[\text{Pf}\{\Gamma(k)\}] = \text{sgn}[\det(H_1(k))] = 1$, therefore $\mathcal{M}$ is solely determined by the sign of $\text{Pf}\{\Gamma(0)\}$. $\text{Pf}\{\Gamma(0)\}$ can be derived analytically from Eq. (7), yielding $\mathcal{M} = \text{sgn}[\mathcal{F}]$, where

$$\mathcal{F} = f_0 - f_1 V_z^2 + 9V_z^4/16, \quad (8)$$

$f_0 = (\bar{\mu}^2 + \Delta_{s3/2}\Delta_{s1/2} - \beta_1^2 - \beta_2^2)^2 + [(\Delta_{s3/2} - \Delta_{s1/2})\bar{\mu} + \beta_1(\Delta_{s3/2} + \Delta_{s1/2})]^2$, $f_1 = \left[10\bar{\mu}^2 + 10\beta_1^2 + 16\beta_1\bar{\mu} + 9\Delta_{s1/2}^2 + \Delta_{s3/2}^2 - 6\beta_2^2\right]/4$, $\beta_1 = \pi^2\gamma_2\left(L_z^{-2} - L_y^{-2}/2\right)$, $\beta_2 = \sqrt{3}\pi^2\gamma_2 L_y^{-2}/2$. Since

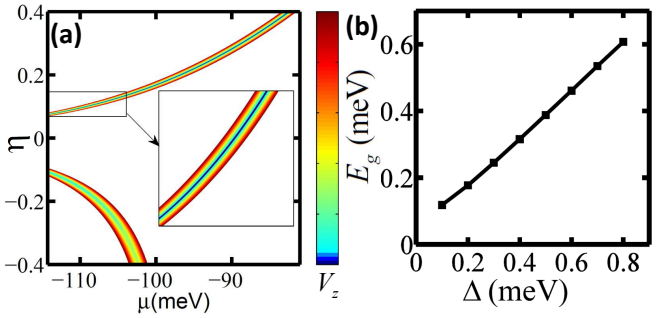

FIG. 2: (a) Plot of the phase boundary ($\mathcal{F}=0$) between topological and non-topological states for different μ, V_z^c and η. $\Delta_{s1/2}=1$ meV, $\beta_2=55.4$ meV (corresponding to $L_y=10$ nm), $\beta_1=(1-\eta)/(2\sqrt{|\eta|})\sqrt{\beta_2^2-\eta\Delta_{s1/2}^2}$. The color region represents the TS state with $\mathcal{M}=-1$. Different colors correspond to different V_z^c. (b) Plot of the minigap E_g versus Δ. $\mu=-50.9$ meV, $V_z=1.5$ meV, $L_y\approx 9$ nm and $L_z\approx 15$ nm.

$\mathcal{M}$ changes sign when $\mathcal{F}$ changes sign, $\mathcal{F}=0$ defines the phase boundary between the topologically trivial and nontrivial states.

When the ratio $\eta=\Delta_{s3/2}/\Delta_{s1/2}\geq\Delta_{s3/2}^2/\beta_2^2$, there exists a magic chemical potential $\bar{\mu}_0=\frac{\eta+1}{4|\eta|}\sqrt{\eta\beta_2^2-\Delta_{s3/2}^2}$ in the heavy hole band such that $f_0=0$, where $\beta_1=(1-\eta)\,\bar{\mu}_0/\,(1+\eta)$. For $f_0=0$, $\mathcal{F}<0$ and Majorana fermions exist even for a vanishingly small V_z. Because $\beta_2^2>>\left|\Delta_{s3/2}\Delta_{s1/2}\right|$ with the strong confinement, $\eta\geq\Delta_{s3/2}^2/\beta_2^2$ is equivalent to that $\Delta_{s3/2}$ and $\Delta_{s1/2}$ have the same sign, in which case the threshold V_z^c for the TS state vanishes. When $\Delta_{s3/2}$ and $\Delta_{s1/2}$ have different signs, V_z^c becomes nonzero, but is still much smaller than that for the electron-doped semiconductors. Therefore the relative signs of the pair potentials should not matter in realistic experiments because a reasonable V_z is always needed to generate a sizable chemical potential region for the TS state. In Fig. 2, we plot the boundary $\mathcal{F}=0$ between topologically trivial and non-trivial states for different μ, V_z^c and η. The TS states for a fixed V_z^c are embraced by two lines with the same color for the corresponding V_z^c. For instance, for $\eta=0.15$ and $V_z^c=1$ meV, Fig. 2 shows that the TS state exists in the region $\mu_1<\mu<\mu_2$ with $\mu_1=-103.3$ meV and $\mu_2=-100.8$ meV. Clearly, the $V_z=0$ line (the center blue line) exists for $\eta>0$, but vanishes for $\eta<0$. When $\eta\to 0^+$, $\bar{\mu}_0\to-\infty$.

The vanishingly small V_z^c for the TS state at $\eta>0$ may also be understood by projecting the four band Luttinger model in Eq. (3) to an effective two heavy hole band model because of the large energy splitting between the heavy and light hole bands. The resulting two band model is generally very complicated for finite k_x and V_z. However, because the Pfaffian is determined by the Hamiltonian at $k=0$ and we are interested in the TS state with vanishingly small V_z, we can do the band projection at $V_z=0$ and around $k_x=0$, leading to an effective pairing $\Delta^{eff}=\left(\Delta_{s3/2}-\kappa\Delta_{s1/2}\right)/\kappa$ and chemical potential $\bar{\mu}_{eff}=\bar{\mu}-\sqrt{\beta_1^2+\beta_2^2}$, with $\kappa=\left(\sqrt{\beta_1^2/\beta_2^2+1}-\beta_1/\beta_2\right)^2$. When $\eta>0$, Δ^{eff} may vanish by choosing $\beta_1/\beta_2=(1-\eta)/2\sqrt{\eta}$, therefore V_z^c also vanishes when $\bar{\mu}_{eff}=0$. While when $\eta<0$, Δ^{eff} is always finite and there is a minimum V_z^c based on Eq. (1) for the two-band model. Note that the zero Δ^{eff} at $k_x=0$ and $V_z=0$ does not imply the zero Δ at a finite V_z and k_x. For a large k_x, the coupling between heavy and light holes becomes important and the mini-gap is finite for a large V_z even at the magic μ_0 (see Fig. 3b).

Henceforth, we consider two representative cases to further illustrate our results: (I) $\Delta_{s3/2}=\Delta_{s1/2}=\Delta$ and (II) $\Delta_{s3/2}=-\Delta_{s1/2}=\Delta$. The corresponding topological region is plotted in Fig. 3a. In the case (I), the TS states exist in the region $|\bar{\mu}-\bar{\mu}_0|\lesssim|V_z|/2$ for both positive and negative V_z. The transition at $V_z=0$ (at which the superconductor is gapless and non-topological) is a quantum transition at which neither the symmetry of the system nor the topological properties change with V_z. Note that the system crosses the phase transition boundary lines twice when V_z changes from $-\infty$ to $+\infty$ for a fixed $\bar{\mu}$, except at $\bar{\mu}_0$. At the phase boundary, the quasiparticle energy gap closes and the superconductor becomes gapless. At $\bar{\mu}_0$, the two lines of the phase boundary merge at $V_z=0$, therefore the superconductor is gapped and topological for all V_z except at $V_z=0$.

In the case (II), the threshold $V_z^c\approx p\Delta$ with $p=2\left[1+2\left(1+\beta_2^2/\beta_1^2\right)^{-1/2}\right]^{-1}$ (see Figs. 3a and 3c). For instance, for hole-doped InAs nanowires (with a typical $g_h^*=35$ [30]) with Nb as the adjacent superconductor ($\Delta\simeq 1$ meV), the required magnetic field B is ~ 0.35 T, which is about 1/3 of the corresponding B for electron-doped InAs nanowires. Therefore, irrespective of the relative sign of $\Delta_{s3/2}$ and $\Delta_{s1/2}$ the threshold B for the TS state in the hole-doped case is much smaller than that in the electron-doped case. The fact that the Majorana fermions can be observed even with a small magnetic field opens the possibility of using a wide range of semiconductor materials with only small g_h^* factors [21, 22].

To further confirm the existence of the Majorana fermions in the above parameter regime, we also numerically solve the BdG equations (5) and obtain the energy spectrum. The Majorana fermion corresponds to a zero energy eigenvalue in the BdG spectrum. Henceforth, we present our results only for the case (I), but have confirmed that the results for the case (II) are similar. In Fig. 3b, we plot the ground and the first excited state energies. The ground state energy becomes zero in the region $\mu_{c_2}<\mu<\mu_{c_1}$, where $\mathcal{M}=-1$ (Fig. 3a). The solution of the BdG equation also yields the minimum energy gap (minigap) above the zero energy states. At this gap and above there are other, finite-energy, states

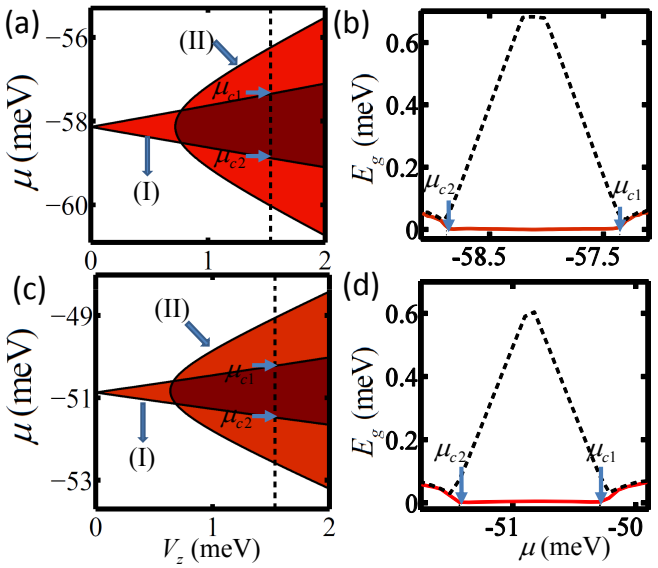

FIG. 3: The parameter regime for Majorana fermions. (a,b) and (c,d) correspond to the single and two band models. $L_y \approx$ 10 nm and $L_z \approx 14$ nm for (b) and case (I) in (a). $L_y \approx$ 9 nm and $L_z \approx 15$ nm for (d) and case (I) in (c). $L_y \approx$ 14.2 nm, $L_z \approx 9.5$ nm for case (II) in (a) and (c). (a,c) are obtained from $\mathcal{M} = -1$ (the filled regions). The widths of the nanowire are chosen to obtain a small V_z^c for each case. (c,d) are obtained from solving the BdG equation with $V_z = 1.5$ meV. $\Delta = 1$ meV. The dashed lines in (b,d) give the minigap.

localized at the end points of the wire. The minigap therefore protects the Majorana states from finite temperature thermal effects. We see that the minigap is of the same order of $\Delta \simeq 1$ meV, which means that the Majorana fermion physics can be accessed at the experimentally accessible temperatures $T < 10$ K.

Effects of multiple confinement bands: In a realistic experiment, multiple confinement energy bands along the y and z directions need be taken into account [18, 31] because they are mixed with each other by the large spin-orbit coupling. Considering the lowest n confinement bands, the BdG Hamiltonian can be written as an $8n \times 8n$ matrix similar as Eq. (5) with $H_1(x)$ replaced with $H_{\rm n}(x) = \int dydz(\phi_1^*(y,z),...\phi_n^*(y,z))^T H_L(\phi_1(y,z),...\phi_n(y,z))$, and Υ with $\Upsilon_n = I_n \otimes \Upsilon$. Here $\phi_i(y,z)$ is the wavefunction on the i-th band in the yz plane. The Nambu spinor basis becomes $\hat{\Psi}(x) = (\hat{\psi}_1(x),\cdots,\hat{\psi}_n(x),\Upsilon\hat{\psi}_1^\dagger(x),\cdots,\Upsilon\hat{\psi}_n^\dagger(x))^T$ with $\hat{\psi}_i(x) = (\hat{\psi}_{\frac{3}{2}i}(x),\hat{\psi}_{\frac{1}{2}i}(x),\hat{\psi}_{-\frac{1}{2}i}(x),\hat{\psi}_{-\frac{3}{2}i}(x))^T$ on the i-th band. We also assume there is no superconducting pairing between holes at different confinement bands, therefore $\Delta_{Sn} = I_n \otimes \Delta_S$. The topological index is found to be $\mathcal{M} = \text{sgn}[\text{Pf}\{\Delta_{Sn}\Upsilon_n\}\text{Pf}\{\Upsilon_n\Delta_{Sn} + H_n^T(k)\Upsilon_n\Delta_{Sn}^{-1}H_n(k)\}]$.

Here we consider only the lowest two relevant energy bands ($l_y = 1$ and 2, $l_z = 1$). In Fig. 3c, we plot the corresponding parameter regime for the TS state, which now has some quantitative difference from that in the one-confinement-band case. However the Majorana fermions can be still realized even with very small Zeeman fields. In Fig. 3d, we plot the energies of the ground and first excited states by solving the relevant multiband BdG equations, which agree with the results obtained from the topological index.

Finally, although the parameter regime for Majorana fermions does not change much as a function of Δ, the minigap has a strong dependence on Δ. In Fig. 2b, we plot the minigap with respect to Δ in the multiband model and find that $E_g \sim \Delta$ (similar as the electron-doped case [15]), instead of Δ^2 as in a regular s-wave or a chiral-p wave superconductor. Therefore the minigap is rather large, which ensures thermal robustness of the Majorana fermions.

Conclusion: We have added a new system, a *hole*-doped nanowire, to the list of systems capable of supporting a non-Abelian TS state. Although the roster is growing, ours is not an ordinary addition. As we have shown here in detail, the requirements (carrier density, magnetic field, g-factor, *etc.*) for the TS state in a hole-doped nanowire are *already accessible in experiments*. Thus this system can be a potential breakthrough facilitating solid-state demonstration of Majorana fermions as well as realization of TQC using a nanowire network.

Acknowledgements: We thank A. Akhmerov, F. Hassler, and M. Wimmer for helpful discussion on the form of the superconducting pairing. This work is supported by DARPA-MTO (FA9550-10-1-0497), DARPA-YFA (N66001-10-1-4025), ARO (W911NF-09-1-0248), and NSF-PHY (1104546).

* Corresponding Author. Email:cwzhang@wsu.edu

[1] G. Moore, and N. Read, Nucl. Phys. B **360**, 362 (1991).
[2] C. Nayak, and F. Wilczek, Nucl. Phys. B **479**, 529 (1996).
[3] N. Read, and D. Green, Phys. Rev. B **61**, 10267 (2000).
[4] S. Das Sarma, M. Freedman, and C. Nayak, Phys. Rev. Lett. **94**, 166802 (2005).
[5] D. A. Ivanov, Phys. Rev. Lett. **86**, 268 (2001).
[6] S. Das Sarma, C. Nayak, and S. Tewari, Phys. Rev. B **73**, 220502(R) (2006).
[7] G. E. Volovik, JETP Lett. **90**, 398 (2009).
[8] M. A. Silaev and G. E. Volovik, J. Low Temp. Phys. **161**, 460 (2010).
[9] S. Tewari *et al.*, Phys. Rev. Lett. **98**, 010506 (2007).
[10] L. Fu, and C. L. Kane, Phys. Rev. Lett. **100**, 096407 (2008); *ibid* **102**, 216403 (2009); A. R. Akhmerov *et al.*, *ibid* **102**, 216404 (2009).
[11] P. A. Lee, arXiv:0907.2681.
[12] C. Nayak *et al.*, Rev. Mod. Phys. **80**, 1083 (2008).
[13] J. D. Sau *et al.*, Phys. Rev. Lett. **104**, 040502 (2010).
[14] J. Alicea, Phys. Rev. B **81**, 125318 (2010).
[15] J. D. Sau *et al.*, Phys. Rev. B **82**, 214509 (2010).
[16] Y. Oreg *et al.* Phys. Rev. Lett. **105**, 177002 (2010).

[17] R. M. Lutchyn, J. D. Sau, and S. Das Sarma, Phys. Rev. Lett. **105**, 077001 (2010).

[18] R. M. Lutchyn, T. D. Stanescu, and S. Das Sarma, Phys. Rev. Lett. **106**, 127001 (2011).

[19] C. Zhang, *et al.* Phys. Rev. Lett. **101**, 160401 (2008).

[20] A. C. Ford *et al.*, Nano Lett., **10**, 509 (2010).

[21] M. Jeppsson *et al.*, J. Crys. Grow. **310**, 5119 (2008).

[22] J. Xiang *et al.*, Nature Nano., **1**, 208 (2006).

[23] S. Das Sarma *et al.*, Phys. Rev. Lett. **94**, 136401 (2005).

[24] J. Sau, S. Tewari, and S. Das Sarma, Phys. Rev. B **85**, 064512 (2012).

[25] B. A. Bernevig, and S.-C Zhang, Phys. Rev. Lett. **95**, 016801 (2005).

[26] T. Stanescu *et al.,* to be published.

[27] A. Yu. Kitaev, Phys. Usp. **44** (suppl.), 131 (2001).

[28] P. Ghosh *et al.*, Phys. Rev. B **82**, 184525 (2010).

[29] An anti-symmetric matrix $A = \begin{pmatrix} R & Q \\ -Q^T & S \end{pmatrix}$ can be diagonalized as $PAP^T = \begin{pmatrix} R & 0 \\ 0 & S + Q^T R^{-1} Q \end{pmatrix}$ with $P = \begin{pmatrix} I & 0 \\ Q^T R^{-1} & I \end{pmatrix}$. Here R, S, Q are matrices, I is a unit matrix.

[30] V. Aleshkin *et al.*, Semiconductors **42**, 828 (2008).

[31] A. C. Potter, and P. A. Lee, Phys. Rev. Lett. **105**, 227003 (2010).